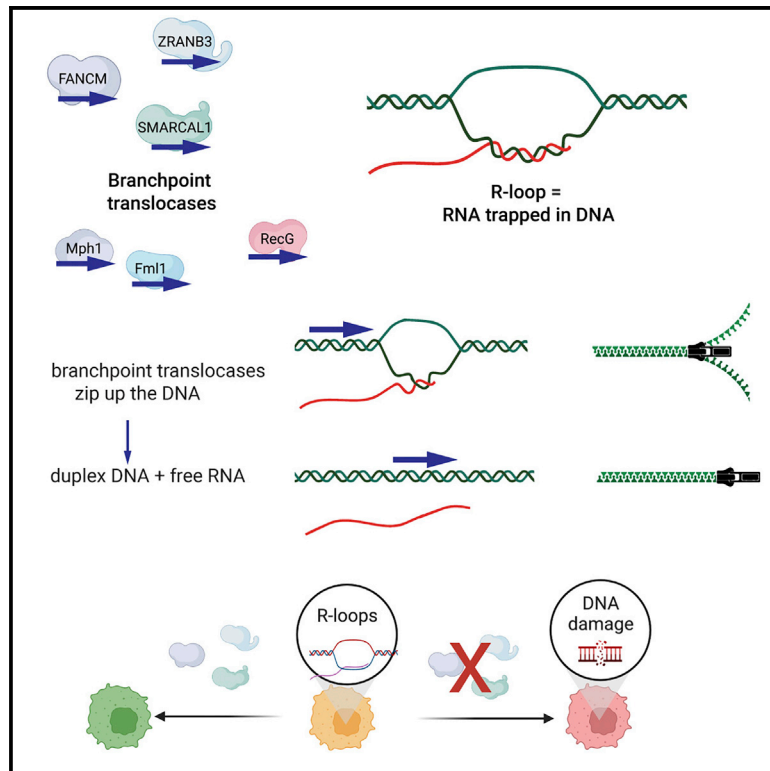


Branchpoint translocation by fork remodelers as a general mechanism of R-loop removal

Graphical abstract



Authors

Charlotte Hodson, Sylvie van Twest, Malgorzata Dylewska, ..., Jörg Heierhorst, Wojciech Niedzwiedz, Andrew J. Deans

Correspondence

adeans@svi.edu.au

In brief

RNA can become trapped in DNA to form stable R loops, which threaten genomic stability. Hodson et al. identify branchpoint translocation as a potent mechanism of R-loop removal. Branchpoint translocases such as FANCM, SMARCAL1, and ZRANB3 are associated with human disease and, additively, suppress R-loop formation and maintain genome stability.

Highlights

- *In vitro* transcription of R-loop-prone loci mimics physiological R-loop formation
- Branchpoint translocation is conserved and distinct from helicase unwinding on R loops
- Human translocases FANCM, SMARCAL1, and ZRANB3 are potent R-loop-removal enzymes
- FANCM, SMARCAL1, and ZRANB3 additively suppress R-loop accumulation and DNA damage



Article

Branchpoint translocation by fork remodelers as a general mechanism of R-loop removal

Charlotte Hodson,^{1,5} Sylvie van Twest,^{1,5} Malgorzata Dylewska,³ Julienne J. O'Rourke,¹ Winnie Tan,¹ Vincent J. Murphy,¹ Mannu Walia,¹ Lara Abbouche,¹ Jadwiga Nieminuszczy,³ Elyse Dunn,¹ Rohan Bythell-Douglas,¹ Jörg Heierhorst,^{2,4} Wojciech Niedzwiedz,³ and Andrew J. Deans^{1,2,6,7,*}

¹Genome Stability Unit, St. Vincent's Institute of Medical Research, Fitzroy, VIC 3065, Australia

²Department of Medicine (St Vincent's Health), University of Melbourne, Fitzroy, VIC 3065, Australia

³The Institute of Cancer Research, London SW3 6JB, UK

⁴Molecular Genetics Unit, St. Vincent's Institute of Medical Research, Fitzroy, VIC 3065, Australia

⁵These authors contributed equally

⁶Lead contact

⁷Twitter: @genomestability

*Correspondence: adeans@svi.edu.au

<https://doi.org/10.1016/j.celrep.2022.111749>

SUMMARY

Co-transcriptional R loops arise from stalling of RNA polymerase, leading to the formation of stable DNA:RNA hybrids. Unresolved R loops promote genome instability but are counteracted by helicases and nucleases. Here, we show that branchpoint translocases are a third class of R-loop-displacing enzyme *in vitro*. In cells, deficiency in the Fanconi-anemia-associated branchpoint translocase FANCM causes R-loop accumulation, particularly after treatment with DNA:RNA-hybrid-stabilizing agents. This correlates with FANCM localization at R-loop-prone regions of the genome. Moreover, other branchpoint translocases associated with human disease, such as SMARCAL1 and ZRANB3, and those from lower organisms can also remove R loops *in vitro*. Branchpoint translocases are more potent than helicases in resolving R loops, indicating their evolutionary important role in R-loop suppression. In human cells, FANCM, SMARCAL1, and ZRANB3 depletion causes additive effects on R-loop accumulation and DNA damage. Our work reveals a mechanistic basis for R-loop displacement that is linked to genome stability.

INTRODUCTION

R loops form when RNA anneals within duplex DNA and displaces a corresponding single-strand DNA (ssDNA) patch. R loops can arise directly from transcription of difficult to transcribe regions or by enzyme-driven integration of RNA, such as R loops created by the Cas9 protein during CRISPR^{1,2} or RAD51AP1 protein during recombination.³ Persistent R loops can be a threat to genome stability because the displaced ssDNA within an R loop is prone to cleavage by nucleases (creating DNA breaks),⁴ recombination with distant DNA sequences (creating chromosome rearrangements)⁵ and atypical modification by ssDNA viral defense proteins such as APOBEC enzymes (creating base substitutions).⁶

R-loop formation in cells can be counteracted by multiple mechanisms. For example, topoisomerase 1 inhibits annealing of RNA to DNA by preventing local unwinding of DNA during transcription.⁷ If RNA does anneal, it can be directly unwound by one of several RNA helicases associated with transcription, such as Senataxin,⁸ UAP56⁹ or Aquarius.¹⁰ In certain circumstances of persistent R-loop formation, RNase H1 can also remove R loops by specifically degrading trapped RNA.¹¹ However, these processes do not entirely prevent R-loop formation. In particular, several studies have shown that DNA-replication-dependent

genome instability is partially prevented when the rate of transcription is reduced, indicating that R loops cause DNA damage predominantly during S phase.^{12–14}

One S-phase-activated pathway of R-loop response is provided by the Fanconi anemia (FA) DNA repair pathway, which culminates in formation of monoubiquitinated FANCD2 at R-loop-rich regions.^{14–16} FANCM is a component of the FA pathway that is essential for activation of FANCD2 ubiquitination¹⁷ in response to the stalling of replication. Stalled replication forks also activate the DNA-structure-specific binding and ATPase activities of FANCM. ATP hydrolysis is coupled to movement of the junction by FANCM across regions of homology to move the branchpoint and, subsequently, remodel the fork by annealing the nascent DNA strands.¹⁸

Human cells contain multiple other “fork remodeler” proteins associated with human disease. These include SMARCAL1 (associated with Schimke immuno-osseous dysplasia¹⁹), ZRANB3 (associated with type 2 diabetes²⁰), and HLTf (associated with colon carcinogenesis²¹). Fork remodelers do not generate ssDNA as an intermediate but take advantage of the complementarity of DNA on either side of a junction (such as those found at stalled DNA replication or transcription bubbles)¹⁷ to displace and reanneal sequences to effect outcomes on DNA junctions. Fork remodelers therefore act by a fundamentally different mechanism



to helicases, and we previously showed that FANCM acts by branchpoint translocation in the unwinding of oligonucleotide-based Flap structures that partially resemble R loops.¹⁴

Here, we show using bona fide R-loop structures that branchpoint translocation is a highly efficient mechanism of R-loop displacement that is affected by multiple enzymes. Human FANCM, SMARCAL1, or ZRANB3 specifically displace RNA from these synthetic R loops and reduce R-loop burden in cells. We show that R-loop removal is an evolutionarily conserved property of the orthologs of fork remodelers in lower eukaryotes (Mph1 from baker's yeast or Fmll from fission yeasts) and bacteria (RecG proteins).^{22–24} Our findings confirm that fork remodelers play a major primary role in R-loop removal that is independent of their role in replication fork remodeling.

RESULTS

***In vitro* unwinding of co-transcriptional R loops by FANCM:FAAP24 complex**

Most previous studies of R-loop-metabolizing enzymes, including our own,^{14,25,26} utilized small oligonucleotide-based structures composed of short regions of RNA annealed to DNA flaps as R-loop mimics. But such structures do not truly resemble co-transcriptional R loops that are known to contain the high GC skew, closed triplex structure, and longer length of native R loops.²⁷ To establish an “ideal R loop” that does incorporate these features of physiological R loops, we used a pUC19 plasmid containing the mouse immunoglobulin class-switch recombination sequence (S_{μ} region) in between a T7 promoter and terminator (Figure S1A). Using T7 polymerase and ³²P-UTP, we generated co-transcriptional R loops using techniques previously described by Roy et al.²⁸ where the formation of R loops can be measured by both a change in plasmid mobility (see on the DNA-stained gels) and retention of the radiolabeled nascent RNA (seen as a slow migrating form on autoradiograph gels) (Figures 1A and 1B). Treatment with RNase H, but not RNase A, led to loss of the R-loop structure on the stained gel and concomitant signal loss on autoradiographs, confirming the presence of RNA-DNA hybrids within the plasmids. RNase H degraded the RNA molecule down to nucleotide-sized fragments (Figure 1B, lane 4).

In contrast to RNase H-mediated RNA degradation, addition of FANCM (as a heterodimer with its stabilization partner FAAP24 in all experiments shown throughout the article) led to release of the RNA transcript without degradation (Figure 1C). This process was ATP dependent: the R loop remained intact when wild-type FANCM-FAAP24 was added in the absence of ATP (Figure 1C, lane 3) or when an ATPase dead FANCM^{K117R} mutant was used (Figure 1C, lane 4).

FANCM unwinds R loops independent of topology, sequence, or replication protein A (RPA) coating

To determine whether specific properties of an R loop governed its ability to be unwound by FANCM, we cloned several sequences previously identified as strongly R-loop prone *in vivo*² into our R-loop test plasmid (Figure S1B) and measured their R-loop-forming potential *in vitro*. The human *APOE*- or *SNRPN*- and mouse *Airn*-genomic loci all formed stable R loops through

purification. These regions were assessed for their percentage of GC skew using *genskew.csb.univie.ac.at* (Figure 1D). In all cases, addition of FANCM:FAAP24 led to rapid and efficient release of the RNA component from the DNA:RNA hybrids without degradation (Figure 1D).

Because RNA bound within an R loop creates underwound or overwound (supercoiled) regions, we also tested the ability of FANCM to displace the RNA from R loops generated with different topological states. First, we used linearization by restriction digestion to remove all covalent topology from the plasmid DNA. This treatment caused no effect on R-loop stability (Figure S2A). Second, we treated R loops with *E. coli* Topo1 or human TopoIII α to generate covalently closed circular (ccc) structures with net zero supercoiling (Figure S2A). Together, these data show that once formed, co-transcriptional ideal R-loop structures are stable regardless of changes in DNA topology. Importantly, FANCM unwound supercoiled, linear, or ccc R loops at essentially equal rates (Figure 1E). This suggests that DNA topology does not affect unwinding activity against native R-loop structures.

We also tested whether RPA influences FANCM activity against R loops (Figure 1G). This is because *in vivo*, the ssDNA displaced within an R loop is most likely bound by ssDNA-binding proteins such as RPA to protect it from attack by DNA-modifying enzymes.¹¹ As expected, a uniform shift in electrophoretic mobility was observed when the displaced DNA strand in the R loop became bound by RPA (Figure S2B). After the addition of FANCM-FAAP24, RPA-bound R loops were also efficiently unwound, albeit at a moderately slower rate than RPA-free substrates (Figure 1G and see also Figure S2C).

Collectively, these data indicate that FANCM-FAAP24 acts in an efficient manner on naked or protein-coated R loops of different sequences and topologies.

FANCM associates with and counteracts excessive R loops in response to transcription stalling agents

To determine whether FANCM is required in cells for suppressing physiological or chemical-induced R-loop formation, we exposed isogenic FANCM-knockout (KO) or parental HCT116 cells (previously characterized by Wang et al.²⁹) to inhibitors of the spliceosome (that promote R loops through retention of intronic sequences) and the topoisomerase 1 inhibitor topotecan (that promotes R loops by stalling transcription).^{14,30,31} Using slot blots of genomic DNA probed with the DNA:RNA-hybrid-specific antibody S9.6, we found a ~30% increase in total R-loop levels in FANCM-deficient cells, similar to that previously observations in HEK293 cells depleted of FANCM by small interfering RNA (siRNA) (Schwab et al.¹⁴). Strikingly, even low concentrations of the two R-loop-promoting compounds dramatically increased the total R-loop levels in FANCM-deficient cells relative to parental cells by up to 600% (Figures 2A, 2B, 2D, and 2E). Moreover, we found that FANCM-deficient cells are particularly sensitive to topotecan and the spliceosome inhibitor pladienolide B (Figures 2C and 2F). In contrast, cells deficient in another FA gene, FANCL (which shared a similar hypersensitivity to the DNA interstrand crosslink-inducing drug acetyl aldehyde with FANCM-deficient cells), were not hypersensitive to these drugs (Figure S3).

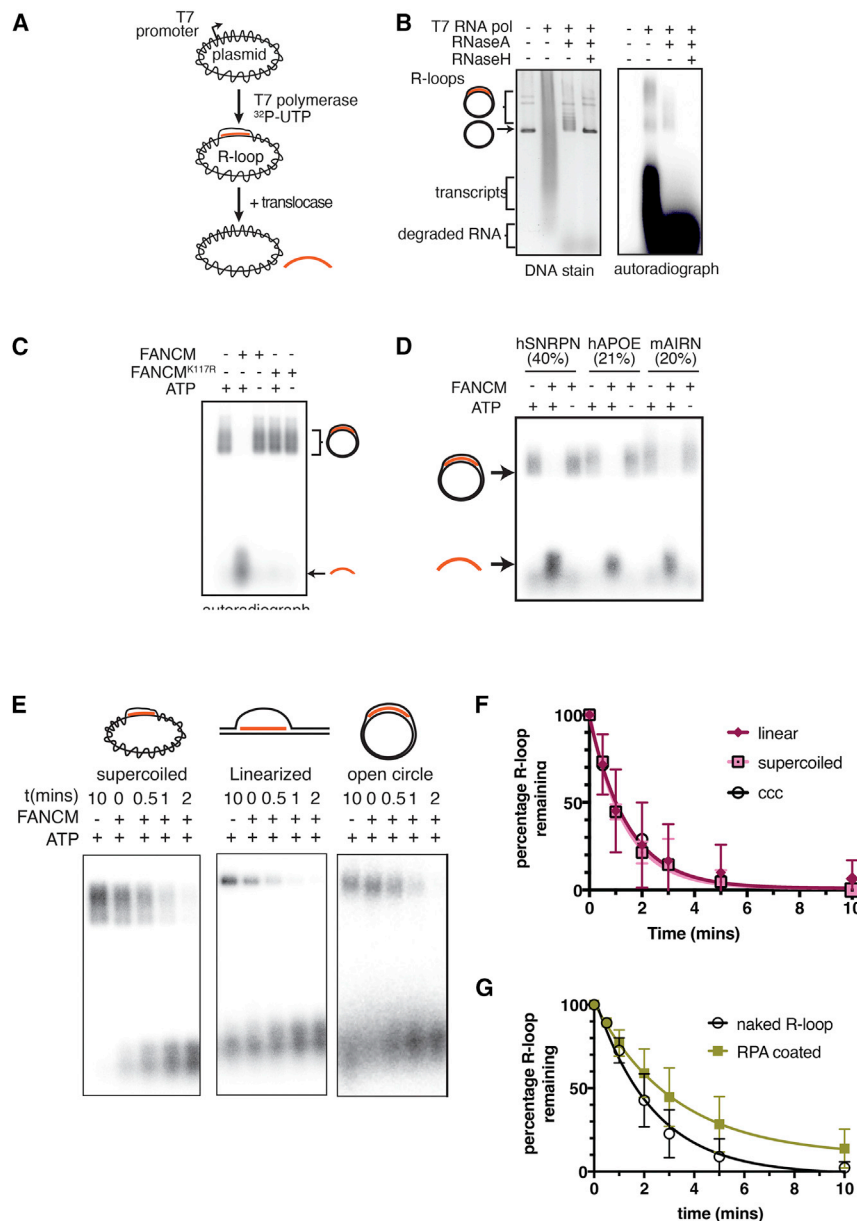


Figure 1. FANCM displaces RNA from R loops of different sequences or structures

(A) Schematic of method used to generate and unwind S_{μ} R loops of different topological states. DNA is colored black and RNA orange.

(B) Plasmid based R loops observed by gel electrophoresis. Sybr gold stain of plasmid DNA molecules reveals the topological changes to the plasmid DNA upon R-loop formation. Right panel is an autoradiograph identifying ^{32}P -UTP incorporation into R loops, transcripts, or post-RNase treatment.

(C) Autoradiograph showing FANCM-FAAP24 (0.25 nM) unwinding purified R loops (1 nM) in an ATP-dependent manner. FANCM^{K117R} is a translocase-activity-deficient mutant.

(D and E) Autoradiographs showing activity FANCM (0.25 nM) on R loops of a different sequence (% indicates GC skew) (D) or topological state (E).

(F and G) Quantification of unwinding activity on different topological states or replication protein A coating (\pm SE) from $n > 3$ experiments. See also Figures S1 and S2.

We noticed that sensitivity to both topotecan and pladienolide B correlated with sharp increases in total cellular R-loop levels in response to these drugs (Figure 2). R-loop levels and LD50 dosage were highly related (compare Figures 2B and 2C and Figures 2D and 2E), suggesting that cellular viability in response to these compounds correlates with a threshold R-loop level. Altogether, these results indicate that FANCM activity in R-loop metabolism is independent of the canonical FA inter-strand crosslink (ICL) repair mechanism to catalytically displace RNA from R loops formed under both physiological and drug-induced conditions.

From these results, two important questions follow: do all R-loop sequences increase after drug treatment, and is FANCM directly associated with specific R-loop-prone loci in

cells? To directly answer this question, we used two different techniques (Figure 2G). First, we used DNA:RNA hybrid immunoprecipitation (DRIP) with the S9.6 antibody and targeted PCR amplification with the S9.6 antibody. At multiple gene promoters, FANCM-deficient cells consistently displayed a 2- to 4-fold increase in DNA:RNA hybrid formation (Figure S3D). This includes at the *SNRPN*, *APOE*, and *RPN* gene promoters that have high GC skew and for which we had shown FANCM activity *in vitro* (Figure 1D). Second, we used chromatin immunoprecipitation (ChIP) with a monoclonal anti-FANCM antibody in wild-type cells after short exposure to topotecan. At the *APOE* and *SNRPN* promoters, both the DRIP signal and the FANCM-ChIP signal showed substantial and consistent increases after drug treatment (Figure 2H).

Together, these findings support the hypothesis that FANCM accumulates at regions of the genome that are prone to R-loop formation. When FANCM is absent, these regions, which include several promoter sequences previously described to be regulated by R-loop levels,² then accumulate to deleterious levels, in turn leading to reduced viability.

R-loop displacement is a conserved feature of fork remodeler proteins

FANCM is a large 230 kDa fork remodeler protein with an N-terminal translocase and branched DNA-binding (junction recognition) domain, a C-terminal ERCC4 structure-specific DNA-binding domain, and multiple protein:protein interaction domains that recruit additional DNA repair factors^{17,32,33} (Figure 3A). These

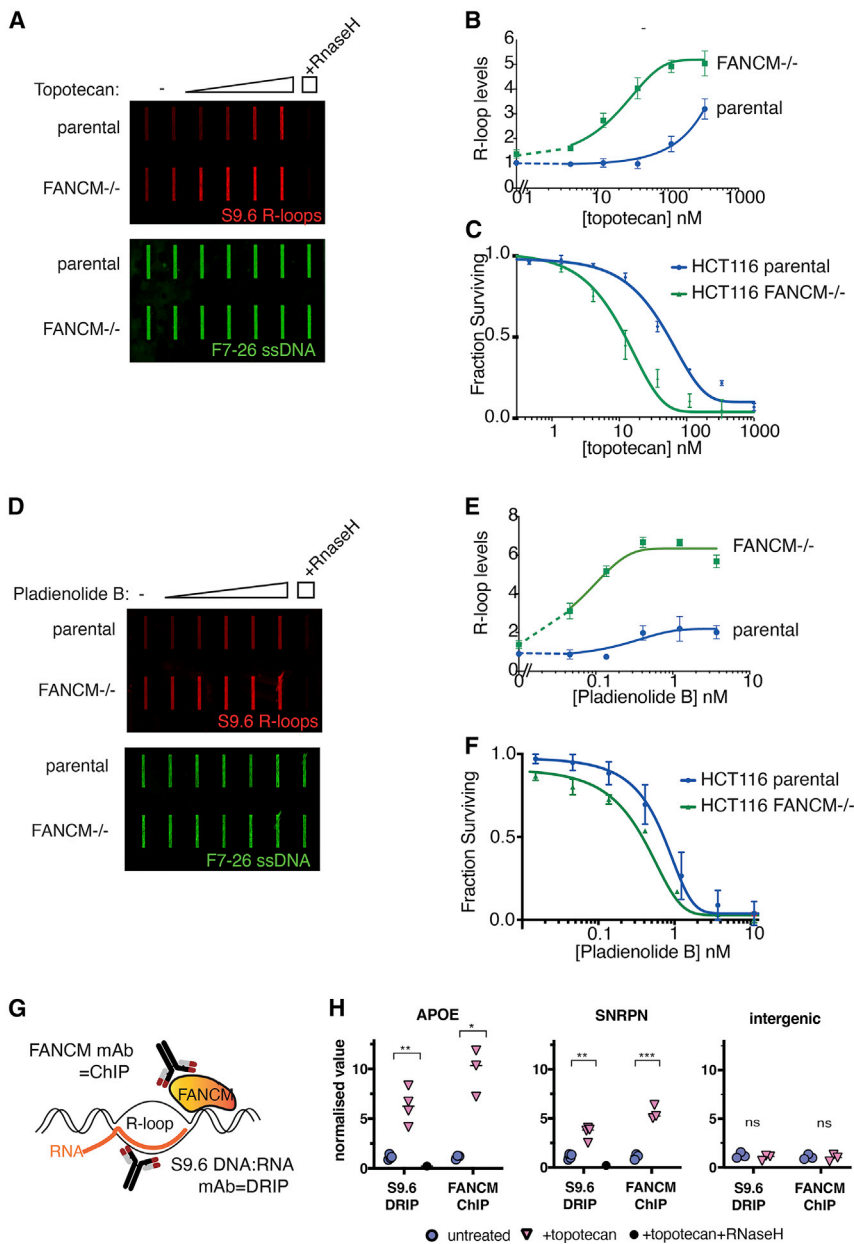


Figure 2. FANCM is necessary for suppression of R-loop formation in cells and resistance to R-loop-promoting agents

(A) Total DNA:RNA hybrid levels in slot blot of HCT116 gDNA after exposure to increasing topotecan. Measured using S9.6 anti-DNA:RNA hybrid or F7-26 anti-DNA. RNase H-treated gDNA was used as a control for S9.6 specificity.

(B) Quantification of S9.6 versus F7-26 slot blot signal from $n = 3$ experiments \pm SE is shown in graphed form (all values normalized to parental untreated).

(C) Dose-response curves of parental and $FANCM^{-/-}$ HCT116 cell lines exposed to topotecan.

(D–F) As in (A)–(C) but after pladienolide B treatment.

(G) Schematic of DRIP and ChIP technique. (H) Enrichment of R loop (S9.6) or FANCM (CE56.1) at APOE or SNRPN promoters compared with an intergenic region after topotecan treatment on $n = 4$ independent experiments (* $p \leq 0.05$, ** $p \leq 0.01$, *** $p \leq 0.001$, **** $p \leq 0.0001$).

FANCM/Mph1/Fml1.^{18,35} RecG also consists of just a translocase and a junction-recognition domain. Based on our findings with $FANCM^{1-800}$, we tested the related homologs, and also found that R-loop unwinding is a conserved feature of yeast and bacterial fork remodelers. Recombinant Mph1, Fml1, or *Thermatoga maritima* RecG all displaced the co-transcriptional R loops with potent activity, indicating a conserved function of FANCM-family proteins (Figure 3C).

But is this R-loop displacement a general property of all helicases and translocases? To begin to answer this question, we tested a panel of human enzymes that had previously been demonstrated to have activity against branched DNA structures. From this panel, two enzymes, ZRANB3 and SMARCAL1, were able to catalyze the displacement of RNA from the R loop with similar efficiency to FANCM protein (Figures 3D and S4). Surprisingly, the

C-terminal parts of the protein are essential for activation of the FA ICL repair pathway but not for cell viability.³⁴ Because we showed that FANCM's role in R-loop suppression is independent of FANCL and the FA ICL repair pathway, we tested the capacity of the FANCM N-terminus ($FANCM^{1-800}$) to unwind R loops. We found $FANCM^{1-800}$ to be sufficient for *in vitro* R-loop removal (Figure 3B), confirming that C-terminal parts of the protein are not required for RNA displacement.

The N-terminal translocase domain of FANCM is also conserved in its orthologs from lower eukaryotes, such as Mph1 from *Saccharomyces cerevisiae* and Fml1 from *S. pombe*.²⁴ Similarly, in bacteria, RecG is a fork remodeler protein that is thought to be the closest prokaryote relative of

related branchpoint translocase HLTF, three junction-specific helicases (BLM, FANCI, and RECQL4), and a phage replicative helicase (gp4) did not show appreciable capacity to unwind the R-loop substrate (Figure 3D). The capacity of each of these enzymes to branch migrate (for translocases) or unwind (for helicases) branched DNA-DNA structures was confirmed in parallel assays (Figure S5 and Castillo-Tandazo et al.³⁶ and Duderstadt et al.^{36,37}). We did observe very weak activity of the BLM helicase and HLTF translocase toward R loops at high enzyme:substrate ratios. For BLM, this is concordant with published studies using oligonucleotide-based DNA:RNA hybrids³⁸ but appears to be ~ 400 -fold less efficient than for FANCM, ZRANB3, and SMARCAL1 in our comparative assays (Figures S5B and S5C).

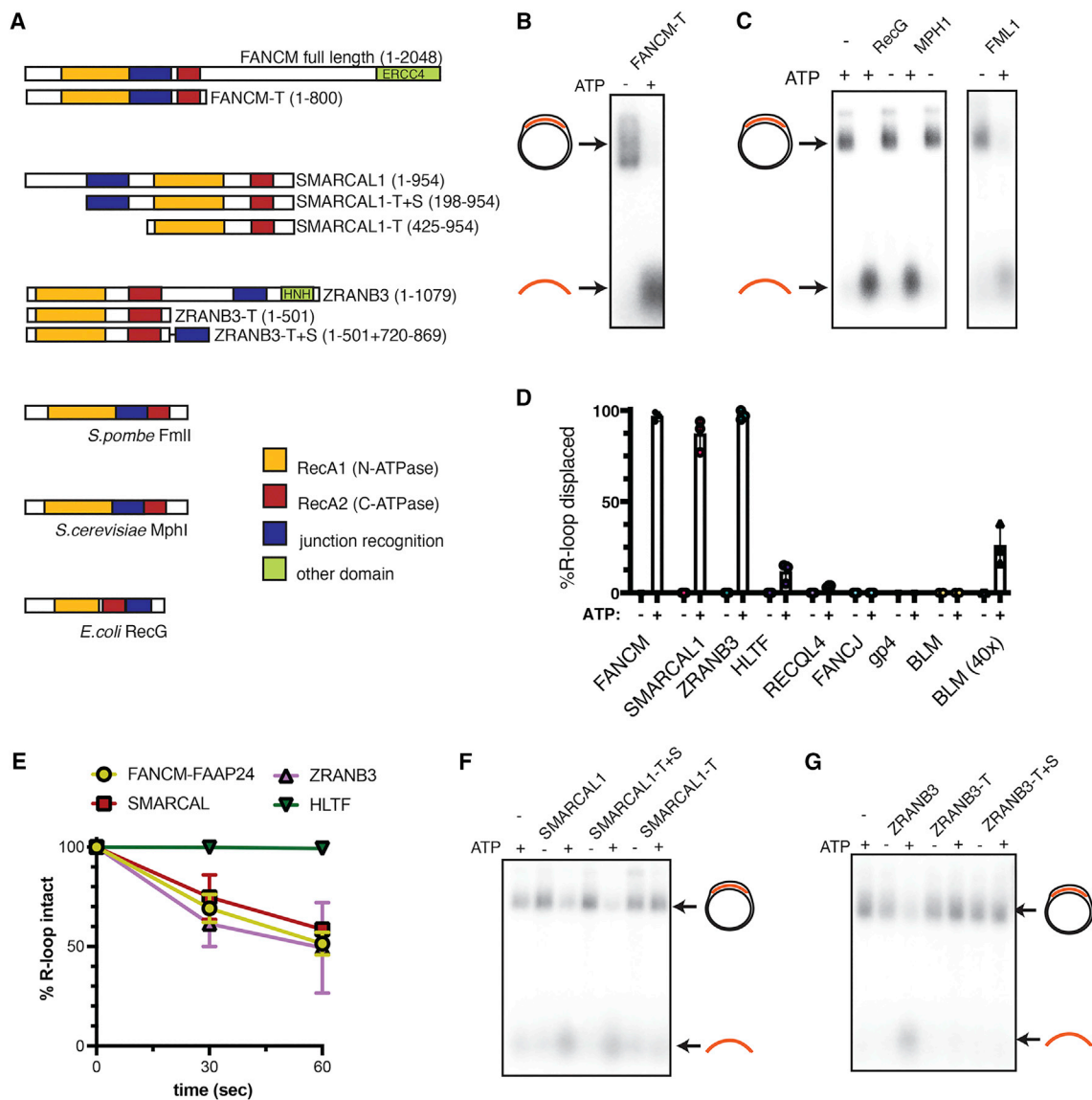


Figure 3. R-loop displacement is a conserved feature of branchpoint translocases

(A) Domain organization of branchpoint translocases showing conserved domains and truncation mutants used in experiments.

(B and C) R-loop displacement assays with (B) FANCM-T (1 nM) and (C) full-length Mph1, Fml1, and RecG (1 nM).

(D) Average unwinding activity in 10 min reactions with indicated translocase/helicase enzymes. BLM shown at 1 or 40 nM, all other enzymes at 1 nM.

(E) R-loop displacement assays with a short time course indicate R-loop-unwinding rates of 10 nM FANCM, SMARCAL1, ZRANB3, or HLTF on plasmid R loops. Results are average \pm SE for $n = 3$ independent experiments.

(F and G) Representative examples (from >3 independent experiments) of experiments conducted with (F) ZRANB3 and ZRANB3 truncations and (G) SMARCAL1 and SMARCAL1 truncations.

In time course experiments, HRLF has negligible activity at concentrations where SMARCAL1, ZRANB3, and FANCM are highly active (Figure 3E). The weak activity of HRLF's branchpoint translocase on R loops may be linked to its unique HIRAN domain, which recognizes the 3'-deoxyribose of nascent DNA and may limit its activity to DNA-only structures.³⁹

We further tested the active branchpoint translocases on RPA-coated R loops. We found that RPA mildly, but reproducibly, activated R-loop displacement by BLM and SMARCAL1, which

contain RPA-binding domains.^{40,41} Conversely, RPA inhibited the activity of ZRANB3, which does not contain an RPA-binding domain (Figure S4D). These findings mirror experiments using purely DNA-based junctions.⁴²

Effective R-loop translocation requires ATPase and junction-recognition domains

While FANCM is thought to be targeted to junction DNA by a junction-recognition insert between its RecA1 and RecA2 folds⁴³

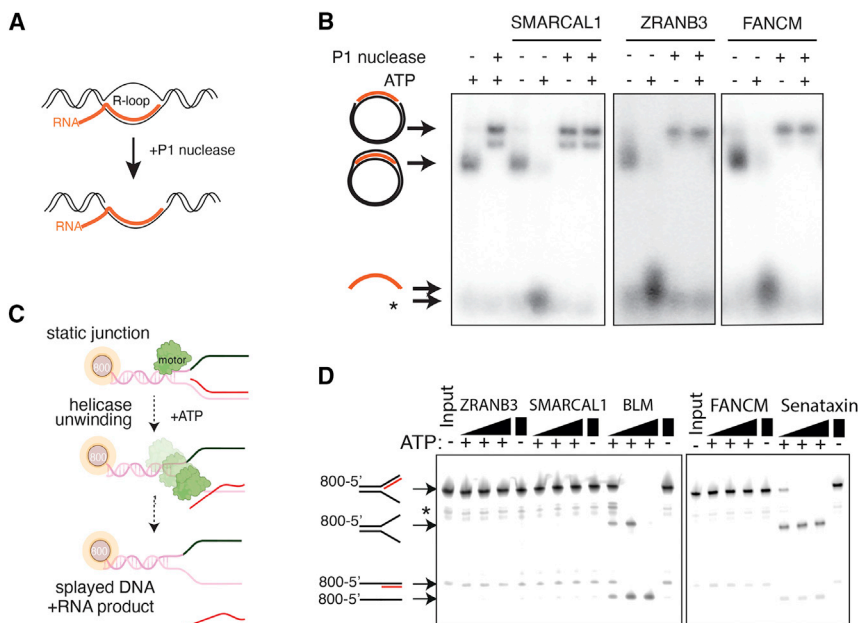


Figure 4. FANCM, SMARCAL1, and ZRANB3 remove R loops by branchpoint translocation and not helicase unwinding

(A) Schematic of how P1 nuclease alters R-loop structure with S9.6 slot blot demonstrating DNA:RNA hybrid is retained after P1 nuclease treatment.

(B) Example activity assays (from $n = 3$) of 1 nM FANCM, ZRANB3, or SMARCAL1 on P1 nuclease-modified R loops compared with unmodified R loops.

(C) Schematic of how helicase activity is necessary for removal of RNA from a static flap structure.

(D) Example activity assays (from $n = 3$ independent experiments) of ZRANB3, SMARCAL1, BLM, FANCM, and Senataxin incubated with static junctions at increasing concentration (1, 5, or 20 nM) \pm 1 mM ATP and separated by PAGE. Only BLM and Senataxin helicases can disrupt this structure. *, truncated Flap structures.

(Figure 4A), SMARCAL1 and ZRANB3 both contain junction-specificity domains outside of their translocase domains^{44,45} as shown in Figure 3A. For SMARCAL1, the junction specification is located in N-terminal HARP domains between residues 226 and 398.⁴⁴ Inclusion of this region together with the core ATPase domain preserved SMARCAL1 activity on both DNA junctions and R loops, while a shorter SMARCAL1 fragment that lacked residues 226–398 was incapable of resolving R loops (Figures 3A, 3E, and S4E).

For ZRANB3, it was previously shown that fusion of this junction-specific domain onto the core translocase region restored branch migration activity.⁴⁵ Using such a fusion, we confirmed this observation on DNA junctions (Figure S4F); however, the same junction was incapable of restoring the activity of truncated ZRANB3 in R-loop dissociation (Figures 3A and 3F). This suggests that an additional domain of ZRANB3 may be required for its activity on DNA:RNA junctions that is not required on purely DNA junctions.

Branchpoint unwinding is dependent upon the existence of a displaced strand

Branchpoint translocation requires the DNA sequences on both sides of a junction to be complementary in order for branch migration to occur.⁴⁶ To confirm that FANCM, ZRANB3, and SMARCAL1 displace RNA solely by branchpoint translocation (and not helicase activity), we used a previously published approach to remove the displaced ssDNA strand within the co-transcriptional plasmid R loops using P1 nuclease (Figure 4A). P1 specifically degrades ssDNA but leaves the double-stranded DNA (dsDNA) and DNA:RNA hybrid component intact.⁴⁷ After treatment with this nuclease, the R loops became resistant to the unwinding activity of FANCM, ZRANB3 or SMARCAL1 (Figure 4B).

Finally, none of the branchpoint translocase enzymes could act on non-migratable “static” Flap structures created from DNA and RNA oligonucleotides (Figures 4C and 4D). This is because the displacement of RNA by branchpoint translocation must be coupled to DNA reannealing, which is not possible when the DNA strands are mismatched (Figure 4C). BLM or Senataxin, enzymes that act instead by a helicase mechanism, can remove RNA from these structures because they do not require unwinding to be coupled with DNA reannealing (Figure 4D). This is a similar result to that observed for purely DNA-based junctions: FANCM, ZRANB3, or SMARCAL1 are not capable of unwinding a non-migratable DNA junction, in contrast to BLM helicase, which can still unwind such structures (Figure S4A).

Combined deletion of branchpoint translocases causes R-loop-dependent genome instability and is deleterious to cellular fitness

Because we discovered that ZRANB3 and SMARCAL1 are similar to FANCM in their activity toward *in vitro* R loops, we used siRNA to deplete these enzymes from cells and examined R-loop accumulation using immunofluorescence. Like we had observed using slot blot experiments for FANCM KO (Figure 2), knockdown of ZRANB3 or SMARCAL1 in HeLa cells resulted in increased R-loop levels (Figure 5A). Moreover, the level of R loops increased further, and was additive on a per cell basis, when ZRANB3 or SMARCAL1 siRNAs were combined with FANCM depletion (Figure 5A). Similar increases in R-loop levels were seen when ZRANB3 or SMARCAL1 siRNAs were used in FANCM-KO HCT116 cells, and DNA:RNA hybrid levels were measured by genomic DNA isolation to exclude the possibility of dsRNA contamination (Figure 5B).

To determine whether these observed synergistic effects on R-loop accumulation also resulted in DNA damage, we

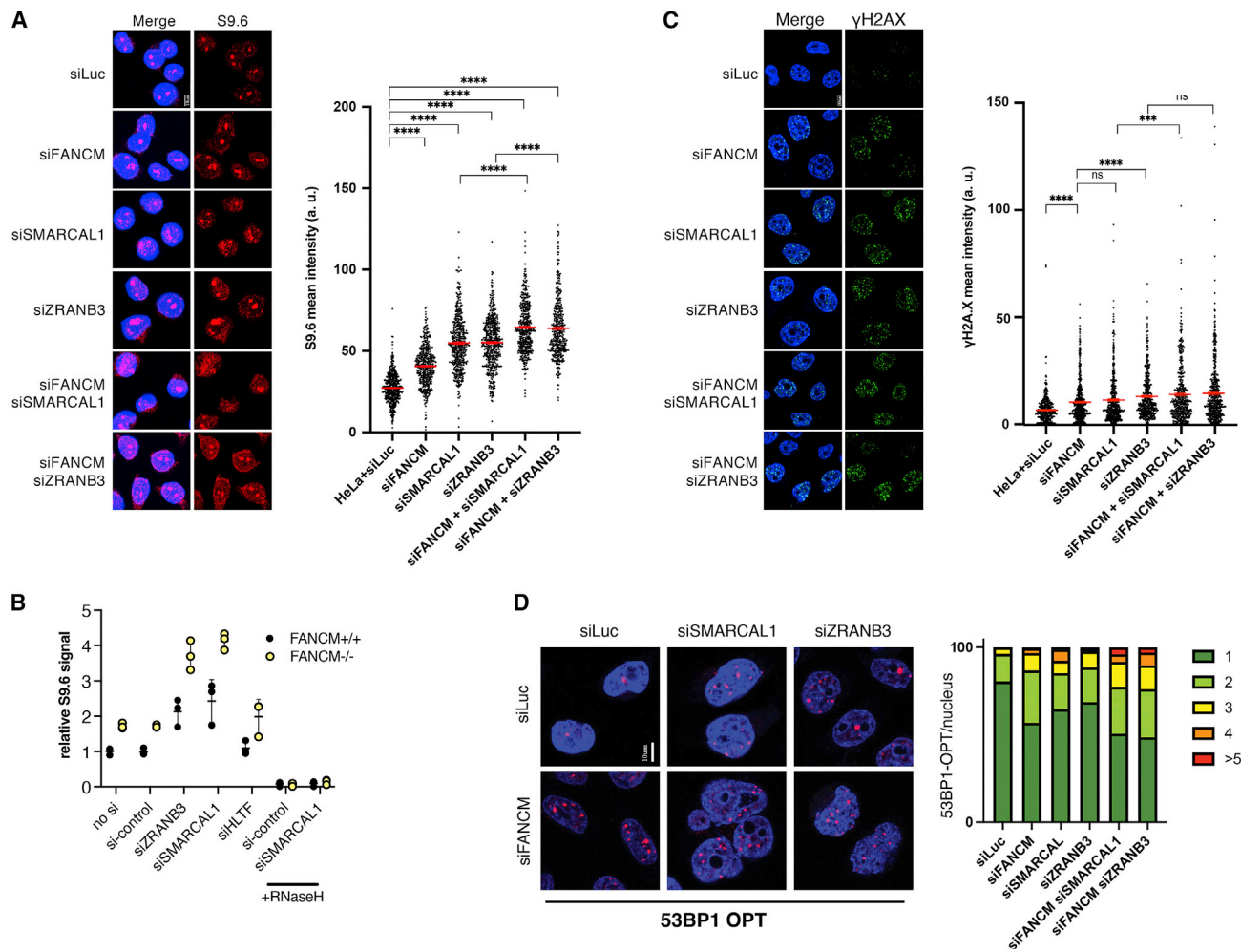


Figure 5. Fork remodelers work cooperatively to suppress R loops and associated markers of genome instability and cell-cycle arrest
(A and B) Example immunofluorescent analysis and quantitative results from 3 independent experiments show (A) elevated R-loop levels detected with S9.6 anti-DNA:RNA hybrid antibody and (B) total DNA:RNA hybrid levels in slot blot of HCT116 gDNA 48 h after indicated siRNA transfection. Measured using S9.6 anti-DNA:RNA hybrid or F7-26 anti-DNA. Results show individual values and averages \pm SE from 3 independent experiments. RNase H-treated gDNA was used as a control for S9.6 specificity.
(C and D) Elevated DNA damage detected with H2AX antibody (C) and elevated 53BP1-OPT domains after HeLa cells were treated with indicated siRNAs (D). Quantifications are shown from overlapping data of 3 independent experiments. A two-tailed Mann-Whitney test was employed to directly compare two groups, (with $\alpha = 0.003$ where Bonferroni correction for 15 multiple comparisons and $***p \leq 0.001$, $****p \leq 0.0001$).

examined several markers. Depletion of any one of the branchpoint translocases caused a 30%–60% increase in the average intensity of γ H2AX, a marker of double-strand break formation (Figure 5C). The increase in damage was independent of any exogenous DNA-damaging agents. Importantly, co-depletion of FANCM and SMARCAL1 (although not ZRNAB3) caused a cumulative average increase in levels of this marker (Figure 5C). The number of intensely stained cells (>25 a.u.) was higher in all the co-depletion conditions. The co-depletion of FANCM and other branchpoint translocases also synergize to increase 53BP1-OPT domains, which mark persistent unrepaired DNA damage transmitted to daughter cells during mitosis (Figure 5D). These findings are consistent with other reports of R-loop increases directly leading to double-strand breaks in DNA.⁶

DISCUSSION

In this work, we describe branchpoint translocation by fork remodelers as a general mechanism for R-loop removal in eukaryotes. R loops that persist during DNA replication present as a potent barrier to the progression of DNA replication.¹³ The fork remodelers FANCM, SMARCAL1, and ZRNAB3 play an overlapping role in the remodeling of replication forks at other types of replication barriers, primarily through translocating the DNA branchpoint of stalled forks to influence replication fork regression and/or restart.^{44,45,48,49} However, our data indicate that these enzymes also share the capacity to directly remove R loops through a similar mechanism of branchpoint translocation. This dual role in displacing R loops and replication fork

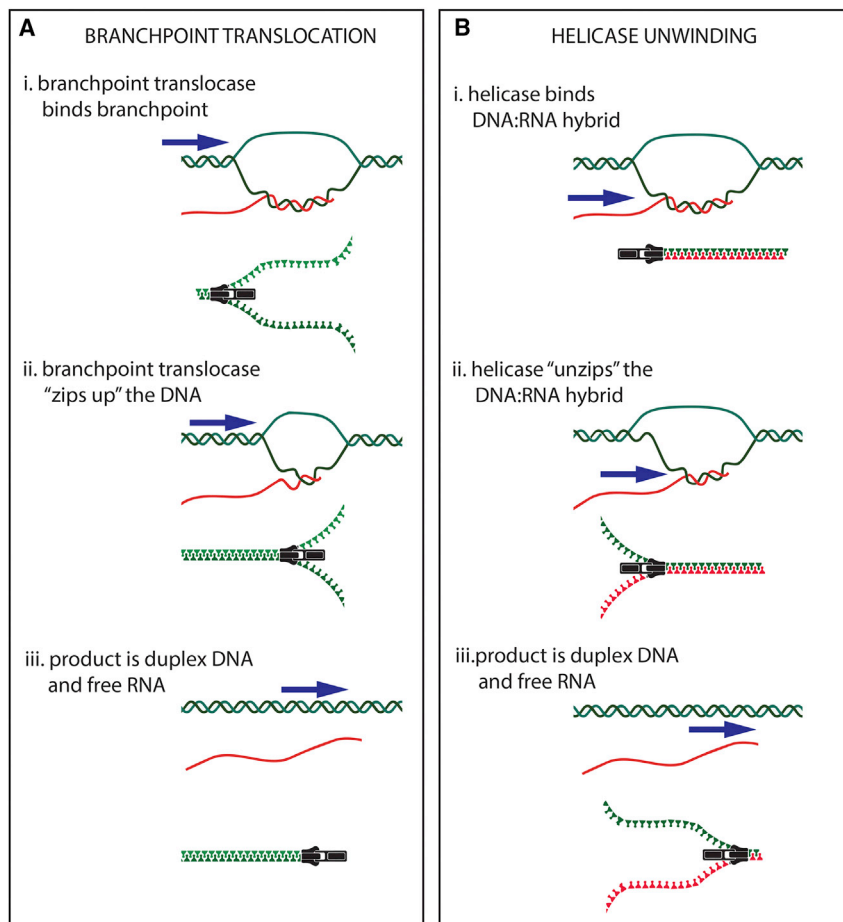


Figure 6. Mechanistic difference between branchpoint translocation and helicase unwinding

(A and B) By analogy with a zipper, branchpoint translocases "zip up" the DNA and thereby indirectly remove RNA (A), whereas helicases "unzip" the DNA:RNA hybrid to achieve the same outcome (B). Location of enzyme action shown by blue arrow. DNA strands shown in green, and RNA strand in red.

We favor the hypothesis that much of the R-loop regulation by branchpoint translocases may be associated with R-loop removal ahead of, or when encountered by, the replication fork. FANCM and the other fork remodelers are enriched in chromatin at sites of ongoing replication,^{32,59} but DNA:RNA hybrids were also recently shown to form by transcription emanating from dsDNA breaks during resection when RNA polymerases become loaded onto broken DNA ends.^{60,61} Fork remodelers may play some role in displacing such hybrids in prevention of over-resection, another phenotype of FANCM-, SMARCAL1-, or ZRANB3-deficient cells.^{32,62} As yet, we also do not know if FANCM, SMARCAL1, and ZRANB3 all act on the same or different R-loop structures. They may act in a common pathway or have substrate preference. For example, on DNA-only-based structures, SMARCAL1, ZRANB3, and

remodeling could potentially allow the enzymes to coordinate the prevention of genome instability caused by collisions between replication and transcription.

Other studies also point to direct influences of fork remodelers on transcription. In particular, cells from patients with Schimke immuno-osseous dysplasia (SIOD) (with homozygous SMARCAL1 deficiency) show genome-wide transcriptional changes¹⁹ and increased DNA:RNA hybrid levels,⁵⁰ and genome-wide ChIP studies revealed that nearly 40% of genomic regions occupied by SMARCAL1 are close to a transcription start site.⁵¹ In mice, SMARCAL1 or ZRANB3 deficiency can alter the transcriptional program (and cancer spectrum) of mice that over-express the c-Myc transcription factor.⁵² R loops have also been shown to accumulate at telomeres after FANCM or SMARCAL1 depletion, particularly in cells that utilize the ALT pathway of telomere maintenance.^{53–55} In *C. elegans*, deletion of the SMRC-1 homolog of SMARCAL1 leads to an accumulation of DNA:RNA hybrids, which is associated with an altered transcription profile and an increase in demethylated histones.⁵⁶ In fruit flies, yeast or bacteria deletion of fork remodelers also leads to elevated R-loop levels associated with both altered transcription and genome instability.^{23,57,58} It is likely that all these phenotypes are associated with the inherent R-loop displacement activity we observed for these enzymes.

FANCM have somewhat different specificities relating to whether the branchpoint is adjacent to either 5' or the 3' single-stranded regions or with or without ssDNA-binding proteins associated.⁶³

The maintenance of genome stability by R-loop removal is regulated by several different RNase nucleases and helicases, which act directly on the DNA:RNA hybrid. Our study identifies another enzyme activity that instead acts on branchpoint translocation of dsDNA adjacent to an R loop to evict trapped RNA. By analogy, we can use zippers to understand the mechanistic difference between branchpoint translocases and helicases (Figure 6). Similar to the opening of a zipper, helicases "unzip" directly the DNA:RNA hybrid, which indirectly allows the DNA to reanneal. In contrast, branchpoint translocases act to "rezip" or "zip up" the DNA—indirectly displacing the RNA as they do so. Because they act on the DNA, branchpoint translocases can simultaneously displace RNA, protein, and annealed DNA (for example, in the recently identified class of pro-recombinogenic molecules called DR loops³) while also reannealing the dsDNA to allow further renewed transcription or DNA replication. A helicase unwinding such structures could potentially leave protein-coated ssDNA regions or topological barriers in its wake. This makes branchpoint translocation a fundamentally more efficient reaction than helicase unwinding. Branchpoint

translocation could allow the RNA displacement to be coupled to other enzymatic activities, making it superior to nuclease degradation (which wastes the RNA transcript).

Although branchpoint translocation is a highly processive property of FANCM, SMARCAL1, and ZRANB3, many other transcription factors and genome-stability proteins contain ATPase and junction-specific DNA- or ssDNA-binding domains. For example, there is emerging evidence that chromatin remodelers are targeted by R loops to regulate the exchange or movement of nucleosomes.^{64,65} It will be interesting to investigate whether these and other enzymes use branchpoint translocation of R loops as a more targeted mechanism of transcription regulation or genome-stability maintenance.

Limitations of the study

While we were able to show co-localization of FANCM and R-loop-prone regions of the genome using ChIP, we were unable to do this for SMARCAL1 or ZRANB3. We tested several commercial antibodies to these proteins and could not find one suitable for the ChIP technique. We have also not tested whether γ H2AX observed after translocase knockdown is localized to where R loops accumulate. Future studies could identify whether particular genome locations or R-loop-prone sequences are regulated uniquely by FANCM, SMARCAL, and ZRANB3 by performing whole-genome ChIP sequencing with novel antibodies, or endogenously tagged versions of these proteins, and determining whether signals co-localize with R loop and γ H2AX peaks.

While we observe total R-loop levels increase on a per-cell basis in all cells (Figure 5A), we have also not determined whether these R loops originate in S phase or whether they accumulate specifically at only one stage of the cell cycle. Future experiments could examine the cell-cycle origin of R loops in translocase-deficient cells by cell synchronization or methods that incorporate cell-stage-specific markers together with R-loop analysis.

STAR★METHODS

Detailed methods are provided in the online version of this paper and include the following:

- KEY RESOURCES TABLE
- RESOURCE AVAILABILITY
 - Lead contact
 - Materials availability
 - Data and code availability
- EXPERIMENTAL MODEL AND SUBJECT DETAILS
- METHOD DETAILS
 - Co-transcriptional R-loop plasmid design and construction
 - R-loop generation and purification
 - Protein purification
 - R-loop unwinding assays
 - Branch migration of RNA flap structures
 - Cell based assays
 - Chromatin and DNA:RNA immunoprecipitation (ChIP and DRIP)
 - Immunofluorescence
- QUANTIFICATION AND STATISTICAL ANALYSIS

SUPPLEMENTAL INFORMATION

Supplemental information can be found online at <https://doi.org/10.1016/j.celrep.2022.111749>.

ACKNOWLEDGMENTS

We thank members of the Genome Stability Unit for input and discussions on the manuscript. Thanks to Lei Li for providing the HCT116 cell lines; Alberto Ciccia for ZRANB3 and SMARCAL1 wild-type (WT) and mutant expression vectors; Antoine van Oijen for gp4; and Steve West for RecG. This work was conducted on Wurundjeri land. This work was funded by National Health and Medical Research Council Australia (grant 1139099), the National Breast Cancer Foundation, and the Victorian Government's OIS Program. Work in W.N.'s laboratory is funded by Cancer Research UK Programme (A24881).

AUTHOR CONTRIBUTIONS

Conceptualization, C.H., J.J.O., and A.J.D.; methodology, C.H., J.J.O., M.D., S.v.T., M.W., V.J.M., and A.J.D.; investigation, all authors.; writing – original draft, C.H. and A.J.D.; writing – review & editing C.H., J.J.O., E.D., M.D., R.B.-D., and A.J.D.; funding acquisition, J.H., W.N., and A.J.D.; supervision, J.H., W.N., C.H., R.B.-D., and A.J.D.

DECLARATION OF INTERESTS

A.J.D. is the recipient of research funding from Tessellate Biosciences and Pfizer, which is unrelated to the work presented. These companies have had no influence on the content of the manuscript.

INCLUSION AND DIVERSITY

We support inclusive, diverse, and equitable conduct of research.

Received: October 2, 2022

Revised: October 5, 2022

Accepted: November 9, 2022

Published: December 6, 2022

REFERENCES

1. Szczelkun, M.D., Tikhomirova, M.S., Sinkunas, T., Gasiunas, G., Karvelis, T., Pschera, P., Siksny, V., and Seidel, R. (2014). Direct observation of R-loop formation by single RNA-guided Cas9 and Cascade effector complexes. *Proc. Natl. Acad. Sci. USA* *111*, 9798–9803. <https://doi.org/10.1073/pnas.1402597111>.
2. Ginno, P.A., Lott, P.L., Christensen, H.C., Korf, I., and Chédin, F. (2012). R-loop formation is a distinctive characteristic of unmethylated human CpG island promoters. *Mol. Cell* *45*, 814–825. <https://doi.org/10.1016/j.molcel.2012.01.017>.
3. Ouyang, J., Yadav, T., Zhang, J.M., Yang, H., Rheinbay, E., Guo, H., Haber, D.A., Lan, L., and Zou, L. (2021). RNA transcripts stimulate homologous recombination by forming DR-loops. *Nature* *594*, 283–288. <https://doi.org/10.1038/s41586-021-03538-8>.
4. Arudchandran, A., Bernstein, R.M., and Max, E.E. (2004). Single-stranded DNA breaks adjacent to cytosines occur during Ig gene class switch recombination. *J. Immunol.* *173*, 3223–3229.
5. Huertas, P., and Aguilera, A. (2003). Cotranscriptionally formed DNA:RNA hybrids mediate transcription elongation impairment and transcription-associated recombination. *Mol. Cell* *12*, 711–721.
6. Sollier, J., and Cimprich, K.A. (2015). Breaking bad: R-loops and genome integrity. *Trends Cell Biol.* *25*, 514–522. <https://doi.org/10.1016/j.tcb.2015.05.003>.
7. Manzo, S.G., Hartono, S.R., Sanz, L.A., Marinello, J., De Biasi, S., Cossarizza, A., Capranico, G., and Chedin, F. (2018). DNA Topoisomerase I

- differentially modulates R-loops across the human genome. *Genome Biol.* 19, 100. <https://doi.org/10.1186/s13059-018-1478-1>.
8. Yüce, Ö., and West, S.C. (2013). Senataxin, defective in the neurodegenerative disorder ataxia with oculomotor apraxia 2, lies at the interface of transcription and the DNA damage response. *Mol. Cell Biol.* 33, 406–417. <https://doi.org/10.1128/MCB.01195-12>.
 9. Pérez-Calero, C., Bayona-Feliu, A., Xue, X., Barroso, S.I., Muñoz, S., González-Basallote, V.M., Sung, P., and Aguilera, A. (2020). UAP56/DDX39B is a major cotranscriptional RNA-DNA helicase that unwinds harmful R-loops genome-wide. *Genes Dev.* 34, 898–912. <https://doi.org/10.1101/gad.336024.119>.
 10. Sollier, J., Stork, C.T., García-Rubio, M.L., Paulsen, R.D., Aguilera, A., and Cimprich, K.A. (2014). Transcription-coupled nucleotide excision repair factors promote R-loop-induced genome instability. *Mol. Cell* 56, 777–785. <https://doi.org/10.1016/j.molcel.2014.10.020>.
 11. Nguyen, H.D., Yadav, T., Giri, S., Saez, B., Graubert, T.A., and Zou, L. (2017). Functions of replication protein A as a sensor of R-loops and a regulator of RNaseH1. *Mol. Cell* 65, 832–847.e4. <https://doi.org/10.1016/j.molcel.2017.01.029>.
 12. Helmrich, A., Ballarino, M., and Tora, L. (2011). Collisions between replication and transcription complexes cause common fragile site instability at the longest human genes. *Mol. Cell* 44, 966–977. <https://doi.org/10.1016/j.molcel.2011.10.013>.
 13. Hamperl, S., Bocek, M.J., Saldivar, J.C., Swigut, T., and Cimprich, K.A. (2017). Transcription-replication conflict orientation modulates R-loop levels and activates distinct DNA damage responses. *Cell* 170, 774–786.e19. <https://doi.org/10.1016/j.cell.2017.07.043>.
 14. Schwab, R.A., Nieminiuszczyc, J., Shah, F., Langton, J., Lopez Martinez, D., Liang, C.C., Cohn, M.A., Gibbons, R.J., Deans, A.J., and Niedzwiedz, W. (2015). The Fanconi anemia pathway maintains genome stability by coordinating replication and transcription. *Mol. Cell* 60, 351–361. <https://doi.org/10.1016/j.molcel.2015.09.012>.
 15. García-Rubio, M.L., Pérez-Calero, C., Barroso, S.I., Tumini, E., Herrera-Moyano, E., Rosado, I.V., and Aguilera, A. (2015). The Fanconi anemia pathway protects genome integrity from R-loops. *PLoS Genet.* 11, e1005674. <https://doi.org/10.1371/journal.pgen.1005674>.
 16. Madireddy, A., Kosiyatrakul, S.T., Boisvert, R.A., Herrera-Moyano, E., García-Rubio, M.L., Gerhardt, J., Vuono, E.A., Owen, N., Yan, Z., Olson, S., et al. (2016). FANCD2 facilitates replication through common fragile sites. *Mol. Cell* 64, 388–404. <https://doi.org/10.1016/j.molcel.2016.09.017>.
 17. Coulthard, R., Deans, A.J., Swuec, P., Bowles, M., McDonald, N.Q., West, S.C., Costa, A., and McDonald, N.Q. (2013). Architecture and DNA recognition elements of the Fanconi anemia FANCM-FAAP24 complex. *Structure* 21, 1648–1658. <https://doi.org/10.1016/j.str.2013.07.006>.
 18. Gari, K., Décaillot, C., Delannoy, M., Wu, L., and Constantinou, A. (2008). Remodeling of DNA replication structures by the branch point translocase FANCM. *Proc. Natl. Acad. Sci. USA* 105, 16107–16112. <https://doi.org/10.1073/pnas.0804777105>.
 19. Boerkoel, C.F., Takashima, H., John, J., Yan, J., Stankiewicz, P., Rosebarker, L., André, J.L., Bogdanovic, R., Burguet, A., Cockfield, S., et al. (2002). Mutant chromatin remodeling protein SMARCAL1 causes Schimke immuno-osseous dysplasia. *Nat. Genet.* 30, 215–220. <https://doi.org/10.1038/ng821>.
 20. Adeyemo, A.A., Zaghloul, N.A., Chen, G., Doumatey, A.P., Leitch, C.C., Hostelley, T.L., Nesmith, J.E., Zhou, J., Bentley, A.R., Shriner, D., et al. (2019). ZFRANB3 is an African-specific type 2 diabetes locus associated with beta-cell mass and insulin response. *Nat. Commun.* 10, 3195. <https://doi.org/10.1038/s41467-019-10967-7>.
 21. Sandhu, S., Wu, X., Nabi, Z., Rastegar, M., Kung, S., Mai, S., and Ding, H. (2012). Loss of HLF function promotes intestinal carcinogenesis. *Mol. Cancer* 11, 18. <https://doi.org/10.1186/1476-4598-11-18>.
 22. Hong, X., Cadwell, G.W., and Kogoma, T. (1995). *Escherichia coli* RecG and RecA proteins in R-loop formation. *EMBO J.* 14, 2385–2392.
 23. Vincent, S.D., Mahdi, A.A., and Lloyd, R.G. (1996). The RecG branch migration protein of *Escherichia coli* dissociates R-loops. *J. Mol. Biol.* 264, 713–721. <https://doi.org/10.1006/jmbi.1996.0671>.
 24. Whitby, M.C. (2010). The FANCM family of DNA helicases/translocases. *DNA Repair* 9, 224–236. <https://doi.org/10.1016/j.dnarep.2009.12.012>.
 25. Chang, E.Y.-C., Novoa, C.A., Aristizabal, M.J., Coulombe, Y., Segovia, R., Chaturvedi, R., Shen, Y., Keong, C., Tam, A.S., Jones, S.J.M., et al. (2017). RECQ-like helicases Sgs1 and BLM regulate R-loop-associated genome instability. *J. Cell Biol.* 216, 3991–4005. <https://doi.org/10.1083/jcb.201703168>.
 26. Shin, J.H., and Kelman, Z. (2006). The replicative helicases of bacteria, archaea, and eukarya can unwind RNA-DNA hybrid substrates. *J. Biol. Chem.* 281, 26914–26921. <https://doi.org/10.1074/jbc.M605518200>.
 27. Ginno, P.A., Lim, Y.W., Lott, P.L., Korf, I., and Chédin, F. (2013). GC skew at the 5' and 3' ends of human genes links R-loop formation to epigenetic regulation and transcription termination. *Genome Res.* 23, 1590–1600. <https://doi.org/10.1101/gr.158436.113>.
 28. Roy, D., Yu, K., and Lieber, M.R. (2008). Mechanism of R-loop formation at immunoglobulin class switch sequences. *Mol. Cell Biol.* 28, 50–60. <https://doi.org/10.1128/MCB.01251-07>.
 29. Wang, Y., Leung, J.W., Jiang, Y., Lowery, M.G., Do, H., Vasquez, K.M., Chen, J., Wang, W., and Li, L. (2013). FANCM and FAAP24 maintain genome stability via cooperative as well as unique functions. *Mol. Cell* 49, 997–1009. <https://doi.org/10.1016/j.molcel.2012.12.010>.
 30. Powell, W.T., Coulson, R.L., Gonzales, M.L., Crary, F.K., Wong, S.S., Adams, S., Ach, R.A., Tsang, P., Yamada, N.A., Yasui, D.H., et al. (2013). R-loop formation at Snord116 mediates topotecan inhibition of Ube3a-antisense and allele-specific chromatin decondensation. *Proc. Natl. Acad. Sci. USA* 110, 13938–13943. <https://doi.org/10.1073/pnas.1305426110>.
 31. Wan, Y., Zheng, X., Chen, H., Guo, Y., Jiang, H., He, X., Zhu, X., and Zheng, Y. (2015). Splicing function of mitotic regulators links R-loop-mediated DNA damage to tumor cell killing. *J. Cell Biol.* 209, 235–246. <https://doi.org/10.1083/jcb.201409073>.
 32. Blackford, A.N., Schwab, R.A., Nieminiuszczyc, J., Deans, A.J., West, S.C., and Niedzwiedz, W. (2012). The DNA translocase activity of FANCM protects stalled replication forks. *Hum. Mol. Genet.* 21, 2005–2016. <https://doi.org/10.1093/hmg/dds013>.
 33. Deans, A.J., and West, S.C. (2009). FANCM connects the genome instability disorders Bloom's Syndrome and Fanconi Anemia. *Mol. Cell* 36, 943–953. <https://doi.org/10.1016/j.molcel.2009.12.006>.
 34. Rosado, I.V., Niedzwiedz, W., Alpi, A.F., and Patel, K.J. (2009). The Walker B motif in avian FANCM is required to limit sister chromatid exchanges but is dispensable for DNA crosslink repair. *Nucleic Acids Res.* 37, 4360–4370. <https://doi.org/10.1093/nar/gkp365>.
 35. Sun, W., Nandi, S., Osman, F., Ahn, J.S., Jakovleska, J., Lorenz, A., and Whitby, M.C. (2008). The FANCM ortholog Fml1 promotes recombination at stalled replication forks and limits crossing over during DNA double-strand break repair. *Mol. Cell* 32, 118–128. <https://doi.org/10.1016/j.molcel.2008.08.024>.
 36. Castillo-Tandazo, W., Smeets, M.F., Murphy, V., Liu, R., Hodson, C., Heierhorst, J., Deans, A.J., and Walkley, C.R. (2019). ATP-dependent helicase activity is dispensable for the physiological functions of Recq4. *PLoS Genet.* 15, e1008266. <https://doi.org/10.1371/journal.pgen.1008266>.
 37. Duderstadt, K.E., Geertsema, H.J., Stratmann, S.A., Punter, C.M., Kulczyk, A.W., Richardson, C.C., and van Oijen, A.M. (2016). Simultaneous real-time imaging of leading and lagging strand synthesis reveals the coordination dynamics of single replisomes. *Mol. Cell* 64, 1035–1047. <https://doi.org/10.1016/j.molcel.2016.10.028>.
 38. Chang, E.Y.-C., Novoa, C.A., Aristizabal, M.J., Coulombe, Y., Segovia, R., Chaturvedi, R., Shen, Y., Keong, C., Tam, A.S., Jones, S.J.M., et al. (2017).

- RECQ-like helicases Sgs1 and BLM regulate R-loop-associated genome instability. *J Cell Biol.* 216, 3991–4005. <https://doi.org/10.1083/jcb.201703168>.
39. Kile, A.C., Chavez, D.A., Bacal, J., Eldirany, S., Korzhnev, D.M., Bezsonova, I., Eichman, B.F., and Cimprich, K.A. (2015). HLTf's ancient HIRAN domain binds 3' DNA ends to drive replication fork reversal. *Mol. Cell* 58, 1090–1100. <https://doi.org/10.1016/j.molcel.2015.05.013>.
40. Bhat, K.P., Bétous, R., and Cortez, D. (2015). High-affinity DNA-binding domains of replication protein A (RPA) direct SMARCAL1-dependent replication fork remodeling. *J. Biol. Chem.* 290, 4110–4117. <https://doi.org/10.1074/jbc.M114.627083>.
41. Shorrocks, A.-M.K., Jones, S.E., Tsukada, K., Morrow, C.A., Belblidia, Z., Shen, J., Vendrell, I., Fischer, R., Kessler, B.M., and Blackford, A.N. (2021). The Bloom syndrome complex senses RPA-coated single-stranded DNA to restart stalled replication forks. *Nat. Commun.* 12, 585. <https://doi.org/10.1038/s41467-020-20818-5>.
42. Bétous, R., Couch, F.B., Mason, A.C., Eichman, B.F., Manosas, M., and Cortez, D. (2013). Substrate-selective repair and restart of replication forks by DNA translocases. *Cell Rep.* 3, 1958–1969. <https://doi.org/10.1016/j.celrep.2013.05.002>.
43. Jiang, F., Ramanathan, A., Miller, M.T., Tang, G.Q., Gale, M., Jr., Patel, S.S., and Marcotrigiano, J. (2011). Structural basis of RNA recognition and activation by innate immune receptor RIG-I. *Nature* 479, 423–427. <https://doi.org/10.1038/nature10537>.
44. Bétous, R., Mason, A.C., Rambo, R.P., Bansbach, C.E., Badu-Nkansah, A., Sirbu, B.M., Eichman, B.F., and Cortez, D. (2012). SMARCAL1 catalyzes fork regression and Holliday junction migration to maintain genome stability during DNA replication. *Genes Dev.* 26, 151–162. <https://doi.org/10.1101/gad.178459.111>.
45. Badu-Nkansah, A., Mason, A.C., Eichman, B.F., and Cortez, D. (2016). Identification of a substrate recognition domain in the replication stress response protein zinc finger ran-binding domain-containing protein 3 (ZNRANB3). *J. Biol. Chem.* 291, 8251–8257. <https://doi.org/10.1074/jbc.M115.709733>.
46. Constantinou, A., Davies, A.A., and West, S.C. (2001). Branch migration and Holliday junction resolution catalyzed by activities from mammalian cells. *Cell* 104, 259–268. [https://doi.org/10.1016/s0092-8674\(01\)00210-0](https://doi.org/10.1016/s0092-8674(01)00210-0).
47. Carrasco-Salas, Y., Malapert, A., Sulthana, S., Molcrette, B., Chazot-Franguiadakis, L., Bernard, P., Chédin, F., Faivre-Moskalenko, C., and Vanoosthuysse, V. (2019). The extruded non-template strand determines the architecture of R-loops. *Nucleic Acids Res.* 47, 6783–6795. <https://doi.org/10.1093/nar/gkz341>.
48. Poole, L.A., and Cortez, D. (2017). Functions of SMARCAL1, ZNRANB3, and HLTf in maintaining genome stability. *Crit. Rev. Biochem. Mol. Biol.* 52, 696–714. <https://doi.org/10.1080/10409238.2017.1380597>.
49. Joseph, S.A., Tagliatalata, A., Leuzzi, G., Huang, J.W., Cuella-Martin, R., and Ciccina, A. (2020). Time for remodeling: SNF2-family DNA translocases in replication fork metabolism and human disease. *DNA Repair* 95, 102943. <https://doi.org/10.1016/j.dnarep.2020.102943>.
50. Pugliese, G.M., Salaris, F., Palermo, V., Marabitti, V., Morina, N., Rosa, A., Franchitto, A., and Pichierrri, P. (2019). Inducible SMARCAL1 knockdown in iPSC reveals a link between replication stress and altered expression of master differentiation genes. *Dis. Model. Mech.* 12, dmm039487. <https://doi.org/10.1242/dmm.039487>.
51. Bansal, R., Hussain, S., Chanana, U.B., Bisht, D., Goel, I., and Muthuswami, R. (2020). SMARCAL1, the annealing helicase and the transcriptional co-regulator. *IUBMB Life* 72, 2080–2096. <https://doi.org/10.1002/iub.2354>.
52. Puccetti, M.V., Adams, C.M., Kushinsky, S., and Eischen, C.M. (2019). Smarcal1 and Zranb3 protect replication forks from myc-induced DNA replication stress. *Cancer Res.* 79, 1612–1623. <https://doi.org/10.1158/0008-5472.CAN-18-2705>.
53. Silva, B., Pentz, R., Figueira, A.M., Arora, R., Lee, Y.W., Hodson, C., Wischnewski, H., Deans, A.J., and Azzalin, C.M. (2019). FANCM limits ALT activity by restricting telomeric replication stress induced by deregulated BLM and R-loops. *Nat. Commun.* 10, 2253. <https://doi.org/10.1038/s41467-019-10179-z>.
54. Cox, K.E., Maréchal, A., and Flynn, R.L. (2016). SMARCAL1 resolves replication stress at ALT telomeres. *Cell Rep.* 14, 1032–1040. <https://doi.org/10.1016/j.celrep.2016.01.011>.
55. Pan, X., Chen, Y., Biju, B., Ahmed, N., Kong, J., Goldenberg, M., Huang, J., Mohan, N., Klosek, S., Parsa, K., et al. (2019). FANCM suppresses DNA replication stress at ALT telomeres by disrupting TERRA R-loops. *Sci. Rep.* 9, 19110. <https://doi.org/10.1038/s41598-019-55537-5>.
56. Yang, B., Xu, X., Russell, L., Sullenberger, M.T., Yanowitz, J.L., and Maine, E.M. (2019). A DNA repair protein and histone methyltransferase interact to promote genome stability in the *Caenorhabditis elegans* germ line. *PLoS Genet.* 15, e1007992. <https://doi.org/10.1371/journal.pgen.1007992>.
57. Morimoto, M., Choi, K., Boerkoel, C.F., and Cho, K.S. (2016). Chromatin changes in SMARCAL1 deficiency: a hypothesis for the gene expression alterations of Schimke immuno-osseous dysplasia. *Nucleus* 7, 560–571. <https://doi.org/10.1080/19491034.2016.1255835>.
58. Lafuente-Barquero, J., Luke-Glaser, S., Graf, M., Silva, S., Gómez-González, B., Lockhart, A., Lisby, M., Aguilera, A., and Luke, B. (2017). The Smc5/6 complex regulates the yeast Mph1 helicase at RNA-DNA hybrid-mediated DNA damage. *PLoS Genet.* 13, e1007136. <https://doi.org/10.1371/journal.pgen.1007136>.
59. Castella, M., Jacquemont, C., Thompson, E.L., Yeo, J.E., Cheung, R.S., Huang, J.W., Sobeck, A., Hendrickson, E.A., and Taniguchi, T. (2015). FANCI regulates recruitment of the FA core complex at sites of DNA damage independently of FANCD2. *PLoS Genet.* 11, e1005563. <https://doi.org/10.1371/journal.pgen.1005563>.
60. Ohle, C., Tesorero, R., Schermann, G., Dobrev, N., Sinning, I., and Fischer, T. (2016). Transient RNA-DNA hybrids are required for efficient double-strand break repair. *Cell* 167, 1001–1013.e7. <https://doi.org/10.1016/j.cell.2016.10.001>.
61. Liu, S., Hua, Y., Wang, J., Li, L., Yuan, J., Zhang, B., Wang, Z., Ji, J., and Kong, D. (2021). RNA polymerase III is required for the repair of DNA double-strand breaks by homologous recombination. *Cell* 184, 1314–1329.e10. <https://doi.org/10.1016/j.cell.2021.01.048>.
62. Tagliatalata, A., Alvarez, S., Leuzzi, G., Sannino, V., Ranjha, L., Huang, J.W., Madubata, C., Anand, R., Levy, B., Rabadan, R., et al. (2017). Restoration of replication fork stability in BRCA1- and BRCA2-deficient cells by inactivation of SNF2-family fork remodelers. *Mol. Cell* 68, 414–430.e8. <https://doi.org/10.1016/j.molcel.2017.09.036>.
63. Halder, S., Ranjha, L., Tagliatalata, A., Ciccina, A., and Cejka, P. (2022). Strand annealing and motor driven activities of SMARCAL1 and ZNRANB3 are stimulated by RAD51 and the paralog complex. *Nucleic Acids Res.* 50, 8008–8022. <https://doi.org/10.1093/nar/gkac583>.
64. Chen, P.B., Chen, H.V., Acharya, D., Rando, O.J., and Fazio, T.G. (2015). R loops regulate promoter-proximal chromatin architecture and cellular differentiation. *Nat. Struct. Mol. Biol.* 22, 999–1007. <https://doi.org/10.1038/nsmb.3122>.
65. Sanz, L.A., Hartono, S.R., Lim, Y.W., Steyaert, S., Rajpurkar, A., Ginno, P.A., Xu, X., and Chédin, F. (2016). Prevalent, dynamic, and conserved R-loop structures associate with specific epigenomic signatures in mammals. *Mol. Cell* 63, 167–178. <https://doi.org/10.1016/j.molcel.2016.05.032>.
66. Vuono, E.A., Mukherjee, A., Vierra, D.A., Adroved, M.M., Hodson, C., Deans, A.J., and Howlett, N.G. (2016). The PTEN phosphatase functions cooperatively with the Fanconi anemia proteins in DNA crosslink repair. *Sci. Rep.* 6, 36439. <https://doi.org/10.1038/srep36439>.

67. Berger, I., Fitzgerald, D.J., and Richmond, T.J. (2004). Baculovirus expression system for heterologous multiprotein complexes. *Nat. Biotechnol.* *22*, 1583–1587. <https://doi.org/10.1038/nbt1036>.
68. Hodson, C., Low, J.K.K., van Twest, S., Jones, S.E., Swuec, P., Murphy, V., Tsukada, K., Fawkes, M., Bythell-Douglas, R., Davies, A., et al. (2022). Mechanism of Bloom syndrome complex assembly required for double Holliday junction dissolution and genome stability. *Proc. Natl. Acad. Sci. USA* *119*, e2109093119. <https://doi.org/10.1073/pnas.2109093119>.
69. Singleton, M.R., Scaife, S., and Wigley, D.B. (2001). Structural analysis of DNA replication fork reversal by RecG. *Cell* *107*, 79–89.
70. Huang, Y., Leung, J.W.C., Lowery, M., Matsushita, N., Wang, Y., Shen, X., Huong, D., Takata, M., Chen, J., and Li, L. (2014). Modularized functions of the Fanconi anemia core complex. *Cell Rep.* *7*, 1849–1857. <https://doi.org/10.1016/j.celrep.2014.04.029>.
71. Henricksen, L.A., Umbricht, C.B., and Wold, M.S. (1994). Recombinant replication protein A: expression, complex formation, and functional characterization. *J. Biol. Chem.* *269*, 11121–11132.
72. Ciccio, A., Nimonkar, A.V., Hu, Y., Hajdu, I., Achar, Y.J., Izhar, L., Petit, S.A., Adamson, B., Yoon, J.C., Kowalczykowski, S.C., et al. (2012). Polyubiquitinated PCNA recruits the ZRANB3 translocase to maintain genomic integrity after replication stress. *Mol. Cell* *47*, 396–409. <https://doi.org/10.1016/j.molcel.2012.05.024>.

STAR★METHODS

KEY RESOURCES TABLE

REAGENT or RESOURCE	SOURCE	IDENTIFIER
Antibodies		
Mouse monoclonal anti- FANCM CV5.1	Inhouse, ⁶⁶	Clone CV5.1
Mouse monoclonal anti- FANCM CE53.1	Inhouse, ⁶⁶	Clone CE53.1
Mouse monoclonal anti- DNA:RNA hybrid S9.6	Purified in house from ATCC hybridoma S9.6	Clone S9.6, RRID: AB_2810829
Mouse monoclonal anti- Flag M2	Sigma Aldrich	Cat # F3165, RRID: AB_259529
Mouse monoclonal anti-SMARCAL1	Santa cruz	Cat# sc376377 RRID: AB_10987841
Rabbit polyclonal anti-ZRANB3	Bethyl	Cat# A303-033A RRID: AB_10773114
Bacterial and virus strains		
NEB-10-beta E.coli	New England Biolabs	Cat#C3019H
Multibac E.coli	Berger et al. ⁶⁷	N/A
BL21-DE3	New England Biolabs	Cat#C2527H
Chemicals, peptides, and recombinant proteins		
Recombinant Flag-FANCM:FAAP24	This paper	N/A
Recombinant Flag-SMARCAL1	This paper	N/A
Recombinant Flag-ZRANB3	This paper	N/A
Recombinant Flag-MPH1	This paper	N/A
Recombinant MBP-BLM	Hodson et al. ⁶⁸	N/A
Recombinant Flag-HLTF	This paper	N/A
Recombinant RecG	Singleton et al. ⁶⁹	N/A
Recombinant gp4	Duderstadt et al. ³⁷	N/A
Recombinant TopIII alpha complex	Hodson et al. ⁶⁸	N/A
Recombinant RecQL4	Castillo-Tandazo et al. ³⁶	N/A
Recombinant RPA trimer	This paper.	N/A
E.coli Topoisomerase I	New England Biolabs	Cat # M0301S
T7 polymerase	New England Biolabs	Cat # M0251L
P1 nuclease	New England Biolabs	Cat # M0660S
Proteinase K	New England Biolabs	Cat # P8107S
RNase H	New England Biolabs	Cat # M0297L
RNase A	Epicentre	Cat #MRNA092
Experimental models: Cell lines		
HCT116 human colorectal carcinoma cell line	ATCC	Cat#CCL-247
HCT116 FANCL-/-	Huang et al. ⁷⁰	N/A
HCT116 FANCM-/-	Wang et al. ²⁹	N/A
High Five <i>Trichoplusia ni</i> cells, also known as BTI-Tn-5B1-4.	Invitrogen	Cat# B85502
Sf9 Spodoptera Frugiperda cells	Cancer Research UK cell line repository	N/A
HeLa human cervical adenocarcinoma cell line	ATCC	Cat#CCL-2
HEK293 human embryonic kidney cell line	ATCC	Cat#CRL-1573
Oligonucleotides		
DsiRNA sequence targeting ZRANB3: UCAAGCAUGGAUCAGACAUCCdAdC	IDT (Singapore)	N/A
DsiRNA sequence targeting SMARCAL1: GCAGAAGAUUCUACGACCUAUUCCdAdG	IDT (Singapore)	N/A

(Continued on next page)

Continued

REAGENT or RESOURCE	SOURCE	IDENTIFIER
DsiRNA sequence targeting HLTf: AAGGAAUUAUAAUGUUAACGAUGAdCdT	IDT (Singapore)	N/A
DsiRNA NC1 non-targetig control sequence	IDT (Singapore)	Cat# 51-01-14-04
DNA oligo XOm1 for non-migratable flap structure: ACGCTGCCGAATTCTACCACTGCCTTGCTAGGACA TCTTTGCCACCTGCAGGTTACCC	IDT (Singapore)	N/A
DNA oligo XOm4 for non-migratable flap structure: CGATAGTCGGATCCTCTAGACAGCTCCATG TAGCAAGGCACTGGTAGAATTCGGCAGCGT	IDT (Singapore)	N/A
RNA oligo XOfap5R: GGGUGAACCUAGCAGG UGGGCAAAGAUGUCC	Bioneer (Australia)	N/A
DNA oligos used for target amplification in ChIP experiments, see Table S1 .	IDT (Singapore)	N/A

Recombinant DNA

pUC19-Mu-switch-R-loop	This paper	Deposited at Addgene #134899
pUC19-mAirm-R-loop	This paper	Deposited at Addgene #134900
pUC19-hAPOE-R-loop	This paper	Deposited at Addgene #134901
pUC19-hSNRPN-R-loop	This paper	Deposited at Addgene #134902
pFL-EGFP-3xFlag-DEST	This paper	Deposited at Addgene #134903
pDONR223-HLTF	Horizon discovery	Clone 100070304
pFL-EGFP-3xFlag-HLTF	This paper	Deposited at Addgene #193055
pADC10-SETXhel	This paper	Deposited at Addgene #193056
pDONR221-Mph1	DNASU plasmid repository	clone 25139
pFL-EGFP-3xFlag-Fml1	This paper	Deposited at Addgene #193058
pET11d-RPA	Henricksen et al. ⁷¹	Addgene # 102616
pFastbac-dual-Flag-FANCM-FAAP24	Coulthard et al. ¹⁷	N/A
pFastbac-dual-Flag-FANCM (K117R)-FAAP24	Coulthard et al. ¹⁷	N/A
pFastbac1-SMARCAL1 and derivatives	Ciccica et al. ⁷²	N/A
pFastbac1-ZRANB3 and derivatives	Ciccica et al. ⁷²	N/A

Software and algorithms

ImageStudio Lite for collection and analysis of LiCor Odyssey images	Li-COR Biosciences	https://www.licor.com/bio/image-studio-lite/
GraphPad Prism for macOS, used for graph generation and statistical analysis	V9.0.1 from GraphPad.	http://graphpad.com

RESOURCE AVAILABILITY

Lead contact

Further information and requests for resources and reagents should be directed to and will be fulfilled by the lead contact, Andrew Deans (adeans@svi.edu.au).

Materials availability

Plasmids generated in this study have been deposited to Addgene (see [key resources table](#)). Other reagents generated in this study will be made available on request, but we may require a completed Materials Transfer Agreement if there is potential for commercial application.

Data and code availability

- Data is available, where not included in the main or supplementary figures, from the [lead contact](#) upon request.
- This paper does not report original code.
- Any additional information required to reanalyze the data reported in this paper is available from the [lead contact](#) upon request.

EXPERIMENTAL MODEL AND SUBJECT DETAILS

Human cell lines (HCT116 and derivatives, HEK239 and HeLa) were cultured in DMEM+10%fetal bovine serum, on tissue culture plasticware, in a humidified chamber at 37°C, 5% CO₂. Cell lines were authenticated by G-banding (Victorian Cytogenetics Service) and STR profiling (Australian Genome Research Facility).

METHOD DETAILS

Co-transcriptional R-loop plasmid design and construction

Co-transcriptional R-loop sequences for the human APOE or SNRPN promoter sequences or murine μ -switch repeat or AIRN promoter sequences were synthesized with a 5'-flanking T7 promoter and 3'-T7-terminator sequence and cloned into the EcoRI and HindIII sites of pUC19 (followed by sequence verification) by Gene Universal (Sequences are provided in [Figure S1](#)). Plasmids were transformed into NEB 10-beta cells (NEB), plated and midi prepped (Qiagen). DNA concentration was established by nanodrop. R-loop forming plasmids have been deposited at Addgene.

R-loop generation and purification

2 μ g of plasmid DNA was incubated in a final reaction volume of 200 μ L containing 1x T7 polymerase reaction buffer (NEB), 25 units of T7 polymerase (NEB), 2.25 mM of each nucleotide CTP, GTP, ATP and 825 nM UTP- α -³²P 3000 Ci/mmol (PerkinElmer) for 1 h at 37°C. The reaction was stopped by heat denaturation at 65°C for 20 mins. 100 μ L of 1.05 M NaCl and 0.03 M MgCl₂ buffer was added to each reaction plus 2.5 μ g of Rnase A (EpiCentre) for 1 hr at 37°C. R-loops were then purified by 2x phenol/chloroform using phase lock tubes (Quanta Bio), precipitated in a final concentration of 0.3 M Na Acetate and 70% ethanol at -20°C overnight. Next day the samples were centrifuged at 13,000 \times g in table top centrifuge for 30 min. Supernatant was removed and samples were washed with 70% ethanol and centrifuged for a further 10 min. Supernatant was removed and pellets were left to air dry. R-loops were resuspended in 10 mM Tris pH8, then ran through 2x S-400 columns (GE Healthcare) to remove unincorporated nucleotides, quantified using nanodrop and stored at 4°C.

Protein purification

The following protein expression protocols were used as previously described:

FLAG-FANCM-FAAP24 and FLAG-FANCM_{K117R}-FAAP24¹⁷: Sf9 insect cells (400 mL) were infected with baculoviruses (MOI = 3) for 60 hr and pelleted at 500 \times g, 4°C. Pellets were washed with 1xPBS. Cells were lysed on ice in 0.5 M NaCl, 0.02 M TEA pH 7.5, 1 mM DTT, 10% glycerol plus mammalian protease inhibitors (Sigma P8340-5 mL) and sonicated on ice 5 \times 10 sec bursts. Lysates were clarified by centrifugation at 35,000G for 40 minutes at 4°C. Clarified supernatant was then incubated with equilibrated Flag M2 resin (Sigma) for 1 hr on a roller at 4°C. Flag resin was then subjected to 3x batch washes with lysis buffer (without mammalian protease inhibitors) with 5 minutes on a roller at 4°C between each spin and 1x wash with lysis buffer containing 1 mM ATP and 3 mM MgCl₂. The resin was then placed into gravity flow column for a final wash and protein was eluted with 100 μ g/ml Flag peptide. Flag elutions containing FANCM were pooled and diluted to have a final concentration of 100 mM NaCl, 20 mM TEA pH7.5, 10% glycerol, 1 mM DTT (buffer B) and added to 400 μ L ssDNA resin overnight on a roller at 4°C. The resin was then placed down gravity flow column and washed with 10CV of buffer B. FANCM-FAAP24 complexes were eluted with buffer B containing 0.5 M NaCl.

RPA,⁷¹ 1 L of induced E.coli BL21-DE2 carrying pETd-RPA were lysed in buffer HI 50 mM KCl, 0.5 M NaSCN + protease inhibitors +800 mM NaCl, followed by centrifugation at 35,000G for 40 minutes at 4°C. Protein was first purified via Affi-Gel blue peak fractionation, then concentrated and applied to hydroxylapatite purification. Protein was then eluted with 4 column volumes of HI buffer containing 80 mM potassium phosphate. The resultant peak fraction was applied to a Mono-Q column in H1 buffer with 100 mM KCl, washed with 3 mL of HI buffer+ 200 mM KCl, and eluted with a gradient of 200-400 mM KCl. Peak fractions were flash frozen and stored at -80C.

MBP-BLM⁶⁸: High Five insect cells (200 mL) were infected with baculoviruses (MOI = 3) for 72 hr and pelleted at 500 \times g, 4°C. Pellets were washed with 1xPBS. Cells were lysed on ice in 0.5 M NaCl, 0.02 M TEA pH 7.5, 1 mM DTT, 10% glycerol plus mammalian protease inhibitors (Sigma P8340-5 mL) and sonicated on ice 5 \times 10 sec bursts. Lysates were clarified by centrifugation at 35,000G for 40 minutes at 4°C. Clarified supernatant was then incubated with equilibrated amylose affinity resin (NEB) for 1 hr on a roller at 4°C. Amylose resin was then subjected to 4x batch washes with lysis buffer (without mammalian protease inhibitors). The resin was then placed into gravity flow column for a final wash and protein was eluted with 20 mM maltose. Maltose elutions containing BLM were pooled and diluted to have a final concentration of 100 mM NaCl, 20 mM TEA pH7.5, 10% glycerol, 1 mM DTT (buffer B). Peak fractions were flash frozen and stored at -80C.

Flag-Topoisomerase III α -RMI1-RMI2⁶⁸ was purified as for Flag-FANCM:FAAP24 but without the ssDNA affinity resin step. Protein was further purified on a Sepax SRT-SEC300 column in 0.5 M NaCl, 0.02 M TEA pH 7.5, 1 mM DTT as the size exclusion running buffer. Peak fractions were concentrated using Viacon filters, flash frozen and stored at -80C.

Flag-SMARCAL1 and Flag-ZRANB3 and their ATPase defective derivatives (D549A/E550A and D157A/E158A respectively) were also purified as described above for FANCM, but without the ssDNA affinity purification step.⁷²

Gateway entry vectors (pDONR) for HLTF (Orfeome v8.1 #100070304), Mph1 (DNASU clone 25,139) and Fml1 (cloned inhouse from *S.Pombe* cDNA) expression vectors were subcloned into pFL-EGFP-3xFlag-DEST baculovirus vectors (Addgene: Plasmid #134903) using Gateway LR clonase II (Thermo). Plasmids were then subsequently integrated into the Multibac Bacmid.⁶⁷ For these proteins, 0.4 L High 5 *Trichoplusia ni* cells (1×10^6 /mL, Invitrogen) were infected with P2 virus (MOI = 2.5). Cells were harvested 72 hours after infection at 500 x g, 4°C and pellets washed with 1xPBS. Cells were lysed on ice in 0.5 M NaCl, 0.02 M TEA pH 7.5, 1 mM DTT, 10% glycerol plus mammalian protease inhibitors (Sigma P8340-5 mL) and sonicated on ice 5 × 10 sec bursts. Lysates was clarified by centrifugation at 35,000G for 40 minutes at 4°C. Clarified supernatant was then incubated with equilibrated Flag M2 resin (Sigma) for 1 hr on a roller at 4°C. Flag resin was then subjected to 4x batch washes with lysis buffer (without mammalian protease inhibitors) with 5 minutes on a roller at 4°C between each spin. The resin was then placed into gravity flow column for a final wash and protein was eluted with 100 µg/ml Flag peptide. Flag-Mph1 and Flag-FANCM-FAAP24 complexes were subjected to further purification by ssDNA affinity resin (Sigma): Flag elutions containing FANCM were pooled and diluted to have a final concentration of 100 mM NaCl, 20 mM TEA pH7.5, 10% glycerol, 1 mM DTT (buffer B) and added to 400 µL ssDNA resin overnight on a roller at 4°C. The resin was then placed down gravity flow column and washed with 10CV of buffer B. FANCM-FAAP24 complexes were eluted with buffer B containing 0.5 M NaCl.

Senataxin-helicase domain (residues 1720–2559) was codon-optimised for expression in *Spodoptera frugiperda* downstream of a dual-insect/human expression promoter (p10-CMV) and the polyhedron 5'-UTR, to generate pADC10-SETXhel (synthesized by Gene Universal). This plasmid was transferred into Multibac bacmid and baculovirus generated. 0.4 L High 5 *Trichoplusia ni* cells (1×10^6 /mL, Invitrogen) were infected with P2 virus (MOI = 3). Cells were harvested 68 hours post infection at 500 x g, 4°C and pellets washed with 1xPBS. Cells were lysed on ice in 50 mM NaCl, 50 mM KCl, 20 mM HEPES pH7.5, 1 mM DTT, 10% glycerol plus mammalian protease inhibitors (Sigma P8340-5 mL) and sonicated on ice 5 × 10 sec bursts. Lysates was clarified by centrifugation at 35,000 x g for 30 minutes at 4°C. Clarified supernatant was then incubated with equilibrated Flag M2 resin (Sigma) and washed and eluted as for proteins above.

Proteins were quantified using BSA titrations on SDS-PAGE gels. All proteins were flash frozen in their final buffers and stored at –80°C. Example Coomassie blue stained SDS-PAGE gels of the purified proteins used in the study are shown in Figure S7. Topoisomerase I from *E.coli*, P1 nuclease and all restriction enzymes were purchased from New England Biolabs.

R-loop unwinding assays

R-loop unwinding reactions (10 µL) contained 0.25 nM of R-loop, 1 mM ATP, 2 µL of protein (protein concentrations stated in main text) in R-loop buffer (6.6 mM Tris pH7.5, 3% glycerol, 0.1 mM EDTA, 1 mM DTT, 0.5 mM MgCl₂) and incubated at 37°C for time as shown in figures. Reactions were stopped by adding 2 µL of stop buffer (10 mg.mL⁻¹ proteinase K (NEB), 1% SDS) and incubated for 15 min at 37°C. 2 µL of 50% glycerol was added to samples prior to loading onto 1% or 0.8% agarose TAE gels, run at 100 V in TAE buffer (40 mM Tris, 20 mM acetic acid, 1 mM EDTA) for 60–90 min. Gels were then crushed between pre-cut biodyene B membranes (Pall) for 1 hour, exposed overnight to a GE phosphor-screen and imaged on a Typhoon scanner (GE Biosciences). To visualize DNA, agarose gels were post stained with Sybr gold (ThermoFisher) 1 in 10,000 in TAE.

Quantification of R-loop unwinding was performed using Image J and Prism software.

Branch migration of RNA flap structures

Migratable or non-migratable RNA flap structures were generated by annealed oligonucleotides, as in,¹⁴ except that DNA was 5'labelled with IRDye-800 (Integrated DNA Technologies), instead of ³²P and results were imaged using LiCor Odyssey.

Cell based assays

HCT116- or FANCM–/– and FANCL–/– derivatives were provided by Lei Li (University of Texas MD Anderson). HEK293 and HeLa cells were from ATCC. Cell lines were authenticated by G-banding (St Vincent's Cytogenetics) and maintained in DMEM + 10% fetal bovine serum at 37°C, 5% CO₂ in a humidified chamber. siRNA was transfected at 10 nM using Dharmafect, 48 hr prior to assay. Sequences corresponding to ZRANB3, SMARCAL1, HLTF, non-targeting control were purchased from IDT (Singapore).

For drug sensitivity assays, cells were plated in 96-well plates at 1,500 cells/well, then treated 24 hrs later with various concentrations of topotecan (aka Hycamptin®, GSK) or pladienolamide B (Calbiochem). After 72 hr, survival was measured using sulforhodamine B assay read at 550 nm on a EnSpire Plate reader (Perkin Elmer).

To measure total cellular R-loop levels, HCT116 cells were treated with drug or vehicle for 4 hr, or siRNA transfection for 48 hr. Total genomic DNA was extracted using Isolate II kit (Bioline). 1 µg of genomic DNA was slot blotted, using a BioRad Microfiltration apparatus, onto Biodyne B Nylon membrane (Thermo Fisher), which was then air-dried and blocked in Odyssey blocking buffer (LiCor). As a control, some samples were treated for 30 mins with RNase H (NEB) prior to blotting. The membrane was then probed with 0.5 µg/mL S9.6 anti-DNA:RNA monoclonal antibody (produced and purified in house from S9.6 hybridoma (ATCC)) and 10 ng/ml anti-DNA (F7-26, Millipore). Atto800-anti-mouse (LiCor) and Cy5-conjugated anti-IgM antibody (Millipore) were used to visualize the level of DNA:RNA hybrids and total DNA detected by the primary antibodies, and visualized and quantified using Odyssey LiCor dual color imaging system and accompanying software.

Chromatin and DNA:RNA immunoprecipitation (ChIP and DRIP)

HCT116 cells (or FANCM-knockout derivatives) were cultured to 70% confluence in 15 cm tissue culture dishes, then treated with topotecan (100 nM or control) for 90 mins. Media was removed and cells fixed in 1% formaldehyde in PBS *in situ* for 30 min. Cross-linking was quenched by incubating cells with 0.125 M glycine diluted in PBS for 10 min at room temperature. After 2x PBS wash, cells were scraped and snap frozen as pellets at -80°C until use. Cell pellets were diluted in 300 μL sonication buffer per 10^6 cells (1% SDS, 10 mM EDTA, 50 mM Tris-HCl pH 8.1 with complete protease inhibitors (Sigma-Aldrich)) and the DNA sheared to lengths between 200 and 800 bp using a UCD-200 Bioruptor (Diagenode, Denville, NJ, USA) on high at 4°C for a total shearing time of 15 min (90 min of 10 s on and 50 s off). Sonicated lysates were centrifuged to remove cell debris and diluted 10-fold in ChIP dilution buffer (0.01% SDS, 1.1% Triton X-100, 1.2 mM ETA, 16.7 mM Tris-HCl pH 8.1, 200 mM NaCl) with protease inhibitors followed by pre-clearance with Protein A beads (Invitrogen) equilibrated with ChIP dilution buffer + 10 mg/ml BSA and 20 $\mu\text{g}/\text{mL}$ of yeast tRNA (Sigma Aldrich, R5636) for 1 h at 4°C on rocker. Supernatants were then separated from beads and a fraction of material retained for input. Chromatin immunoprecipitation was performed using 5 μg mouse anti-FANCM (clone CE56.1,⁶⁶) overnight at 4°C with gentle mixing. DNA:RNA hybrid immunoprecipitation was performed using 10 μg anti-DNA:RNA hybrid (clone S9.6) for 2 hr at 4°C with gentle mixing. A separate control was pre-treated with RNaseH (NEB) for 1 hr at 37°C . Beads were washed one time each with Low Salt buffer (0.1% SDS, 1% Triton X-100, 2 mM EDTA, 20 mM Tris-HCl pH 8.1, 150 mM NaCl), High Salt buffer (0.1% SDS, 1% Triton X-100, 2 mM EDTA, 20 mM Tris-HCl pH 8.1, 500 mM NaCl) and LiCl buffer (0.25 M LiCl, 1% NP40, 1% deoxycholate, 1 mM EDTA, 10 mM Tris-HCl pH 8.1), followed by two washes with TE buffer. Protein-DNA complexes were eluted from the beads (0.1 M NaHCO_3 , 1% SDS) at RT for 30 min with two rounds of elution. Protein was digested by incubation with 50 $\mu\text{g}/\text{mL}$ of proteinase K at 45°C for 1 hr. DNA was purified by two extractions with phenol:chloroform:isoamyl alcohol and ethanol precipitation. FANCM and S9.6 bound and input samples were analysed by qPCR using primers that amplify R-loop prone regions of the genome or a negative control region (Table S1).

Immunofluorescence

For the R-loops detection cells were grown on coverslips overnight before siRNA transfection. Cells were washed with PBS, fixed with ice-cold methanol for 10 min, permeabilized with ice-cold acetone for 1 min, washed with PBS and blocked for 1 h at RT in 3% BSA and 0.1% Tween 20 in 4x SSC buffer. For primary immunolabeling, cells were incubated in blocking buffer with S9.6 antibody (1:500; mouse) for 3 h at RT. Cells were then washed three times with PBS followed by incubation with Alexa Fluor 555-conjugated secondary antibody (1:500, Invitrogen) in blocking buffer for 1 h at RT followed by 3 washes of PBS. Once dried, Vectashield (with DAPI staining) on coverslip were applied. Images were acquired using Leica SP8 laser scanning confocal microscope with LasX software on 63x objective. Image analysis was carried out with FIJI (ImageJ) software.

To visualize γH2AX and 53BP1 foci, cells were fixed with 4% paraformaldehyde for 10 min and permeabilized with 0.2% Triton X-100 for 10 min. After blocking in 10% FBS in PBS, cells were incubated with anti- γH2AX (1:500, mouse, Millipore) or anti-53BP1 (1:1000, mouse Millipore), followed by incubation with the secondary antibody and then mounted.

QUANTIFICATION AND STATISTICAL ANALYSIS

Graphing and statistical analysis was performed using Graphpad Prism software. Statistical details of experiments can be found in the figure legends of relevant results. Significance was defined in all experiments with an alpha of 0.05, except when multiple comparisons were performed in non-parametric tests and Bonferroni corrections were used.